Published in final edited form as:
Angew Chem Int Ed Engl. 2009 ; 48(20): 3622–3626. doi:10.1002/anie.200900863.

A Synthetic High-Spin Oxoiron(IV) Complex. Generation, Spectroscopic Characterization and Reactivity**

Dr. Jason England,
Department of Chemistry and Center for Metals in Biocatalysis, University of Minnesota, 207 Pleasant St. SE, Minneapolis, MN 55455 (USA), Fax: (+1) 612-624-7029

Dr. Marlène Martinho,
Department of Chemistry, Carnegie Mellon University, Pittsburgh, PA 15213 (USA)

Erik R. Farquhar,
Department of Chemistry and Center for Metals in Biocatalysis, University of Minnesota, 207 Pleasant St. SE, Minneapolis, MN 55455 (USA), Fax: (+1) 612-624-7029

Jonathan R. Frisch,
Department of Chemistry and Center for Metals in Biocatalysis, University of Minnesota, 207 Pleasant St. SE, Minneapolis, MN 55455 (USA), Fax: (+1) 612-624-7029

Dr. Emile L. Bominaar[Prof.],
Department of Chemistry, Carnegie Mellon University, Pittsburgh, PA 15213 (USA)

Dr. Eckard Münck[Prof.], and
Department of Chemistry, Carnegie Mellon University, Pittsburgh, PA 15213 (USA)

Dr. Lawrence Que Jr.[Prof.]
Department of Chemistry and Center for Metals in Biocatalysis, University of Minnesota, 207 Pleasant St. SE, Minneapolis, MN 55455 (USA)

Eckard Münck: emunck@cmu.edu; Lawrence Que: larryque@umn.edu

Keywords

bioinorganic chemistry iron-oxo; nonheme iron complexes; high-valent compounds; enzyme models

High-valent oxoferryl intermediates have been proposed as the active oxidants in the catalytic cycles of a wide range of mononuclear non-heme oxygen activating enzymes.[1] These high-valent species have now been spectroscopically characterized for four enzymes and were found in all instances to contain high-spin ($S = 2$) iron(IV) centers.[2] Contemporaneously, the first examples of the existing family of synthetic nonheme oxoiron(IV) complexes were characterized,[3–5] which are exclusively octahedral and in all but one case exhibit the $S = 1$, rather than $S = 2$, spin-state. Given that DFT suggests higher reactivity for an $S = 2$ oxoiron(IV) unit,[6,7] it is perhaps not surprising that there is a scarcity of such complexes. Indeed, the only example to date is $[Fe^{IV}(O)(H_2O)_5]^{2+}$ (**1**),

**This work was supported by grants from the NIH (GM-33162 to LQ and EB-001475 to EM) and the NSF (CHE070073 to ELB through TeraGrid resources provided by the NCSA). X-ray crystallographic data collection and structure solution were performed by Dr. Victor G. Young, Jr. at the X-Ray Crystallographic Laboratory, Department of Chemistry, University of Minnesota. XAS data were collected on beamline X3B at the National Synchrotron Light Source and beamline 7-3 at the Stanford Synchrotron Lightsource, both of which are supported by the U.S. DOE and NIH.

Correspondence to: Emile L. Bominaar; Eckard Münck, emunck@cmu.edu; Lawrence Que, Jr., larryque@umn.edu.

which is generated by reacting $[Fe^{II}(H_2O)_6]^{2+}$ with ozone in acidic aqueous solution.[8a] Complex **1** has a $t_{1/2}$ of only 7 s at 25 °C,[8b] and the aqueous medium limits our options for significantly lengthening its lifetime by working at low temperature (T < 0 °C). We have consequently sought an alternative approach to obtain an S = 2 oxoiron(IV) complex.

Consideration of the crystal field splitting diagram for an octahedral oxoiron(IV) complex reveals that the spin state is determined by the gap between the d_{xy} and the d_{x2-y2} orbitals.[7] In the nitrogen-donor supported S = 1 complexes reported thus far, this gap is larger than the spin pairing energy. Therefore, weakening the strength of the equatorial ligand field is an obvious strategy to obtain S = 2 complexes, a principle demonstrated by the tetraaqua ligand set of **1**.[8] An alternative approach is to adopt a trigonal bipyramidal (TBP) geometry, where the d_{xy} and d_{x2-y2} orbitals would become degenerate. Thus a tetradentate tripodal ligand with sufficient steric constraints to enforce local C_{3v} symmetry at the iron(II) center could afford, upon introduction of an axial oxo ligand, a trigonal bipyramidal oxoiron(IV) complex with an S = 2 ground state. Such a geometry is found for the oxoiron(III) complex of the tris(ureaylato) ligand employed by Borovik.[9] This complex was obtained from the reaction of its iron(II) precursor with O_2 and proposed to derive from the reduction of an initially formed oxoiron(IV) species, but direct evidence for the latter has to date not been obtained. TMG_3tren (Figure 1A) is another example of such a ligand,[10] which has recently found use in the successful stabilization of a superoxocopper(II) complex and its subsequent structural characterization.[11] Furthermore, the high level of steric encumbrance provided by TMG_3tren should inhibit intermolecular decay processes, thereby stabilizing the highly reactive Fe^{IV}=O unit.

Combination of equimolar amounts of TMG_3tren and $Fe^{II}(OTf)_2(CH_3CN)_2$ in THF afforded $[Fe^{II}(TMG_3tren)(OTf)](OTf)$ (**2**), whose crystal structure (Figure 1B)[12] exhibited the desired TBP geometry (τ = 0.96 [13]). Reaction of **2** in CH_3CN with 1 equiv 2-(*tert*-butylsulfonyl)iodosylbenzene ($^tBuSO_2C_6H_4IO$)[14] led to the formation of an orange complex **3** ($t_{1/2}$ = 4.3 h at –30°C; $t_{1/2}$ ≈ 30 sec at 25°C) with absorption maxima λ_{max} (ε_{max}) centered at 400 (9800), 825 (260) and 866 (250) nm (Figure 2, main). An electrospray mass spectrum of **3** exhibited peaks at *m/z* = 661.3 and 256.2, with isotope distribution patterns consistent with their respective formulation as $\{[Fe^{IV}(O)(TMG_3tren)](OTf)\}^+$ and $[Fe^{IV}(O)(TMG_3tren)]^{2+}$ (Figure S1 and Figure S2). The presence of an Fe=O unit in **3** was confirmed by resonance Raman spectroscopy, which revealed a vibration at 843 cm^{-1} that shifted to 810 cm^{-1} upon ^{18}O-labelling of **3** (Figure 2, inset). This vibrational frequency and isotope shift ($\Delta\nu_{theoretical}$ ≈ 37 cm^{-1}) are both consistent with its assignment as ν(Fe=O). Furthermore, the ^{19}F-NMR spectrum of **3** displayed a single resonance at −79.9 ppm, which corresponds to free triflate. This observation coupled with the fact that **3** exhibits the same UV-vis spectrum in both coordinating (CH_3CN) and non-coordinating (CH_2Cl_2) solvents indicates that no exogeneous ligands bind to the iron center and that by extension the 5-coordinate geometry found in **2** is retained in **3**, leading us to formulate the latter as $[Fe^{IV}(O)(TMG_3tren)]^{2+}$.

Mössbauer spectroscopy demonstrates that **3** has an S = 2 iron(IV) center. The zero field spectrum of Figure 3A exhibits a doublet with quadrupole splitting, ΔE_Q = −0.29 mm/s, and isomer shift, δ = 0.09 mm/s. The observation of a doublet at 4.2 K indicates that **3** has integer electronic spin. The δ-value is strongly indicative of an iron(IV) complex, and although the value of δ is distinctly lower than those for **1** (0.38 mm/s)[8a] and TauD-**J** (0.30 mm/s),[15c] it is similar to that of the Fe^{IV} site of $[Fe^{IV}(O)(6\text{-}Me_3TPA)(\mu\text{-}O)Fe^{III}(6\text{-}Me_3\text{-}TPA)(H_2O)]$ (0.10 mm/s; 6-Me_3-TPA = tris(6-methylpyridyl-2-methyl)amine),[17] reflecting the nitrogen-rich ligand environment of **3**. Approximately 88% of the Fe in the

Supporting information for this article is available on the WWW under http://www.angewandte.org or from the author.

sample belongs to **3**. A minor high-spin Fe^{III} contaminant accounts for the remaining absorption (Figure S3). In applied magnetic fields, the spectra of **3** exhibit paramagnetic hyperfine structure. Fitting these spectra with an $S = 2$ spin Hamiltonian yields a parameter set that compares well with other high-spin oxoiron(IV) systems (Table 1). In contrast, analyzing the data by assuming an $S = 1$ center yields an unacceptable A-tensor, with an $A_{iso} = (A_x + A_y + A_z)/3 \approx -29.0$ T that is nearly twice as large as A_{iso} values reported for $S = 1$ complexes.[4, 5, 16, 18] Moreover, the spin-dipolar part of the A-tensor, $\boldsymbol{A} - A_{iso}$, would be about four times smaller than observed for $S = 1$ Fe^{IV}=O complexes.

The Fe K-edge X-ray absorption spectrum of **3** reveals an edge energy of 7123.2 eV (vs 7121.1 eV for **2**) and a pre-edge peak assigned to 1s→3d transitions with an area of 27 units (Figure 4 top), both features being within the range of values found for the synthetic Fe^{IV}=O complexes previously studied.[16,19] In contrast to the pre-edge features of existing $S = 1$ complexes that can be modelled with a single Gaussian, the pre-edge region of **3** contains two discernible features at 7113.8 and 7115.6 eV that have areas of 24 and 3 units, respectively (Figure S4, Table S1). This phenomenon was predicted in a recent DFT study and was rationalized in terms of a splitting of the α and β d_z^2 orbitals by spin polarization, which is expected to be significantly larger in the $S = 2$ case.[20] EXAFS analysis for **3** (Figure 4 bottom) yields a best-fit (Table S2) with an O/N scatterer at 1.65 Å, assigned to the Fe=O unit, and a further shell of 4 O/N-scatterers at 1.99 Å, corresponding to the N-donors of the supporting ligand. This Fe=O distance is essentially the same as that found crystallographically for other oxoiron(IV) complexes.[4,18,21]

DFT calculations performed on **3** further support our $S = 2$ spin-state assignment. Geometry optimization yields a structure with C_3 symmetry (Figure 1C) and an Fe=O bond length of 1.648 Å, in close agreement with that obtained from the EXAFS analysis. In contrast, the Fe-N_{ave} distance of 2.055 Å obtained from DFT is significantly longer than that found by EXAFS. Complex **3** has a ^{5}A ground state with the four d electrons in two half-filled E levels (Table S3), with the lowest $S = 1$ and $S = 0$ configurations calculated to be respectively ~10,000 cm^{-1} and ~12,000 cm^{-1} above the $S = 2$ ground state. Notably, the calculated Mössbauer parameters (ΔE_Q, δ and the spin-dipolar contribution to the A-tensor) are in excellent agreement with the experimental data (Table 1). The small value for ΔE_Q results from cancellation of valence against ligand contributions, the latter arising from donation of electron density from the oxo ligand into the vacant E{d_{xz}, d_{yz}} and empty A{d_z^2} orbitals of the iron. Lastly, the calculated spin populations at the iron and the oxo group are +3.08 and +0.64, respectively, similar to the results obtained for **1** and TauD-**J**. [8a, 15c]

The oxidative reactivity of **3** has been investigated with several substrates and the second order rate constants derived from these studies in CH_3CN solution at −30°C are listed in Table 2, alongside those of the well studied $S = 1$ complexes $[Fe^{IV}(O)(TMC)(CH_3CN)]^{2+}$ (**4**) [4,16,22] and $[Fe^{IV}(O)(N4Py)]^{2+}$ (**5**, N4Py = bis(2-pyridylmethyl)bis(2-pyridyl)-methylamine).[21,23] Complex **3** acts as a stoichiometric oxo-transfer agent to PPh_3, but behaves as a 1-e^- oxidant in reactions with dihydroanthracene (DHA) and 1,4-cyclohexadiene (CHD), with 2 equiv **3** yielding 1 equiv anthracene and benzene, respectively. In general, **3** is a more active oxidant than **4**, but comparable to **5**. Surprisingly, **3** oxidizes DHA thirteen times more slowly than CHD, despite there being no significant difference in the oxidation rates of these two substrates by either **4** or **5**. Since DHA and CHD have similar C-H bond dissociation energies,[24] the large rate difference observed for **3** suggests that the TMG_3tren ligand impedes access of the bulkier DHA to the Fe=O unit (Figure 1D and Figure S5). Such sterically-derived mitigation of reactivity has been observed for other tetramethylguanidinyl-ligated systems.[25] Lastly, the use of DHA-d_4 as substrate for **3** afforded a kinetic isotope effect (KIE) of 18, which is above the semi-

classical limit of 7. Thus, as for the $S = 2$ oxoferryl enzymatic intermediates[1] and the $S = 1$ complexes **4** and **5**,[22,23] there is a significant contribution from hydrogen atom tunneling in C-H bond cleavage by **3**.

In this communication we have described the high-yield synthesis of an $S = 2$ oxoiron(IV) complex, making it amenable for full spectroscopic characterization. Complex **3** resembles TauD-**J** in several respects (Table 1). Both **3** and TauD-**J** exhibit a near-UV charge transfer band that is likely to be associated with an oxo-to-iron(IV) charge transfer transition, as excitation into these bands results in the observation of resonance enhanced Fe=O vibrations.[15a] The charge transfer band of **3** is red-shifted relative to that of TauD-**J**, in line with the greater Lewis acidity expected for an oxoiron(IV) unit supported by the neutral TMG_3tren ligand, instead of the dianionic bis(carboxylato)-containing coordination sphere of TauD-**J**.[2a,15c] Differences in coordination environment are also reflected in the Mössbauer parameters. Interestingly, **3** exhibits an oxidative efficacy that is merely comparable to that of the $S = 1$ complex **5** (Table 2), rather than exceeding it, which appears to belie the prevailing DFT-derived consensus that the $S = 2$ manifold is inherently more reactive than the corresponding $S = 1$ state.[6,7] This attenuation in the reactivity of **3** most likely derives from the protection of the high-spin oxoiron(IV) moiety afforded by the sterically bulky TMG_3tren ligand, a design strategy we have successfully employed here to attain the elusive $S = 2$ spin-state. Further ligand tuning may allow access to more reactive $S = 2$ oxoiron(IV) model complexes that might provide invaluable insight into the inherent reactivity and spectroscopic properties of these key biologically relevant entities.

Experimental Section

2: A solution of TMG_3tren (0.55 g, 1.25 mmol) in THF (10 mL) was added to a Schlenk flask charged with $Fe(OTf)_2(CH_3CN)_2$ (0.54 g, 1.25 mmol) and the resultant mixture stirred overnight. The cream-colored precipitate obtained was isolated by filtration, washed with THF (3 × 5 mL) and diethyl ether (2 × 15 mL), and dried under vacuum to give an off-white colored powder (0.97 g, 93 %) that analyzed as a mono-acetonitrile adduct. Anal. Calcd. (found) for $C_{25}H_{51}F_6FeN_{11}O_6S_2$: C, 35.93 (35.89); H, 6.15 (6.21); N, 18.44 (18.24). The acetonitrile-free title compound was obtained as a pale yellow crystalline solid (0.84 g, 85 % overall) by vapor diffusion of diethyl ether into a concentrated dichloromethane solution of the acetonitrile solvate. ^{1}H-NMR (CD_3CN, all peaks appear as broad singlets): δ 213.2 (3H, CH_2), 86.7 (3H, CH_2), 61.7 (3H, CH_2), 34.3 (9H, N*Me*), 20.9 (9H, N*Me*), 9.9 (9H, N*Me*), 1.3 (3H, CH_2), −13.6 (9H, N*Me*). MS (+ESI): *m/z* 645.1 [(M-OTf)$^+$], 248.1 [{M-(OTf)$_2$}$^{2+}$]. Anal. Calcd. (found) for $C_{23}H_{48}F_6FeN_{10}O_6S_2$: C, 34.76 (34.67); H, 6.09 (6.19); N, 17.63 (17.51).

3(OTf)$_2$: Solutions of the orange-colored complex **3** were obtained by reaction of a CH_3CN, or CH_2Cl_2, solution of **2** with one equivalent of ^{t}Bu$SO_2C_6H_4IO$,[14] dissolved in CH_2Cl_2. Solutions of oxidant up to a concentration of 60 mM were routinely used.

References

1. Krebs C, Fujimori D. Galonic, Walsh CT, Bollinger JM Jr. Acc. Chem. Res. 2007; 40:484. [PubMed: 17542550]
2. a) Price JC, Barr EW, Tirupati B, Bollinger JM Jr, Krebs C. Biochemistry. 2003; 42:7497. [PubMed: 12809506] b) Hoffart LM, Barr EW, Guyer RB, Bollinger JM Jr, Krebs C. Proc. Natl. Acad. Sci. U. S. A. 2006; 103:14738. [PubMed: 17003127] c) Eser BE, Barr EW, Frantom PA, Saleh L, Bollinger JM Jr, Krebs C, Fitzpatrick PF. J. Am. Chem. Soc. 2007; 129:11334. [PubMed: 17715926] d) Galonic DP, Barr EW, Walsh CT, Bollinger JM Jr, Krebs C. Nat. Chem. Biol. 2006; 3:113. [PubMed: 17220900]
3. Que L Jr. Acc. Chem. Res. 2007; 40:493. [PubMed: 17595051]

4. Rohde J-U, In J-H, Lim MH, Brennessel WW, Bukowski MR, Stubna A, Münck E, Nam W, Que L Jr. Science. 2003; 299:1037. [PubMed: 12586936]
5. Lim MH, Rohde J-U, Stubna A, Bukowski MR, Costas M, Ho RYN, Münck E, Nam W, Que L Jr. Proc. Natl. Acad. Sci. U. S. A. 2003; 100:3665. [PubMed: 12644707]
6. a) Hirao H, Kumar D, Que L Jr, Shaik S. J. Am. Chem. Soc. 2006; 128:8590. [PubMed: 16802826] b) Bernasconi L, Louwerse MJ, Baerends EJ. Eur. J. Inorg. Chem. 2007:3023.
7. Decker A, Rohde J-U, Klinker EJ, Wong SD, Que L Jr, Solomon EI. J. Am. Chem. Soc. 2007; 129:15983. [PubMed: 18052249]
8. a) Pestovsky O, Stoian S, Bominaar EL, Shan X, Münck E, Que L Jr, Bakac A. Angew. Chem., Int. Ed. 2005; 44:6871. *Angew. Chem.***2005**, *117*, 7031; b) Pestovsky O, Bakac A. J. Am. Chem. Soc. 2004; 126:13757. [PubMed: 15493935]
9. MacBeth CE, Golombek AP, Young VG Jr, Yang C, Kuczera K, Hendrich MP, Borovik AS. Science. 2000; 289:938. [PubMed: 10937994]
10. Wittmann H, Raab V, Schorm A, Plackmeyer J, Sundermeyer J. Eur. J. Inorg. Chem. 2001:1937.
11. Wurtele C, Gaoutchenova E, Harms K, Holthausen MC, Sundermeyer J, Schindler S. Angew. Chem., Int. Ed. 2006; 45:3867. *Angew. Chem.***2006**, *118*, 3951.
12. Single-crystal structure and refinement data for **2**: $C_{23}H_{48}F_6FeN_{10}O_6S_2$, M_w = 794.68, monoclinic, space group $P2_1/c$, a = 12.6127(17), b = 15.273(2), c = 18.880(3) Å, α = 90, β = 94.573(2), γ = 90°, V = 3625.3(8) $Å^3$, Z = 4, ρ_{calcd} = 1.456 $Mg{\cdot}m^{-3}$, $Mo_{K\alpha}$ radiation (λ = 0.71073 Å, μ = 0.612 mm^{-1}), T = 173(2) K. A total of 7417 (R_{int} = 0.0353) independent reflections with 2θ < 26.39° were collected. The resulting parameters were refined to converge at R_1 = 0.0465 (I > 2θ) for 518 parameters on 7417 independent reflections (wR_2 = 0.1390). Max./min. residual electron density 0.977/−0.493 $eÅ^{-3}$; GOF = 1.114. Further experimental details are provided in the Supporting Information. CCDC 714035 contains the supplementary crystallographic data for this paper. These data can be obtained free of charge from The Cambridge Crystallographic Data Centre via www.ccdc.cam.ac.uk/data_request/cif
13. Addison AW, Rao TN, Reedijk J, Van Rijn J, Verschoor GC. J. Chem. Soc., Dalton Trans. 1984:1349.
14. Macikenas D, Skrzypczak-Jankun E, Protasiewicz JD. J. Am. Chem. Soc. 1999; 121:7164.
15. a) Proshlyakov DA, Henshaw TF, Monterosso GR, Ryle MJ, Hausinger RP. J. Am. Chem. Soc. 2004; 126:1022. [PubMed: 14746461] b) Riggs-Gelasco PJ, Price JC, Guyer RB, Brehm JH, Barr EW, Bollinger JM Jr, Krebs C. J. Am. Chem. Soc. 2004; 126:8108. [PubMed: 15225039] c) Sinnecker S, Svensen N, Barr EW, Ye S, Bollinger JM Jr, Neese F, Krebs C. J. Am. Chem. Soc. 2007; 129:6168. [PubMed: 17451240]
16. Jackson TA, Rohde J-U, Seo MS, Sastri CV, DeHont R, Stubna A, Ohta T, Kitagawa T, Münck E, Nam W, Que L. J. Am. Chem. Soc. 2008; 130:12394. [PubMed: 18712873]
17. Zheng H, Yoo SJ, Münck E, Que L Jr. J. Am. Chem. Soc. 2000; 122:3789.
18. Thibon A, England J, Martinho M, Young VG, Frisch JR, Guillot R, Girerd J-J, Münck E, Que L Jr, Banse F. Angew. Chem., Int. Ed. 2008; 47:7064. *Angew. Chem.***2008**, *120*, 7172.
19. Rohde J-U, Torelli S, Shan X, Lim MH, Klinker EJ, Kaizer J, Chen K, Nam W, Que L Jr. J. Am. Chem. Soc. 2004; 126:16750. [PubMed: 15612713]
20. Berry JF, DeBeer George S, Neese F. Phys. Chem. Chem. Phys. 2008; 10:4361. [PubMed: 18654674]
21. Klinker EJ, Kaizer J, Brennessel WW, Woodrum NL, Cramer CJ, Que L Jr. Angew. Chem., Int. Ed. 2005; 44:3690. *Angew. Chem.***2005**, *117*, 3756.
22. Chivukula SV, Lee J, Oh K, Lee YJ, Lee J, Jackson TA, Ray K, Hirao H, Shin W, Halfen JA, Kim J, Que L Jr, Shaik S, Nam W. Proc. Natl. Acad. Sci. U.S.A. 2007; 104:19181. [PubMed: 18048327]
23. Kaizer J, Klinker EJ, Oh NY, Rohde J-U, Song WJ, Stubna A, Kim J, Münck E, Nam W, Que L Jr. J. Am. Chem. Soc. 2004; 126:472. [PubMed: 14719937]
24. Luo, Y-R. Comprehensive Handbook of Chemical Bond Energies. CRC Press; 2007.
25. Herres-Pawlis S, Verma P, Haase R, Kang P, Lyons CT, Wasinger EC, Floerke U, Henkel G, Stack TDP. J. Am. Chem. Soc. 2009; 131:1154. [PubMed: 19119846]

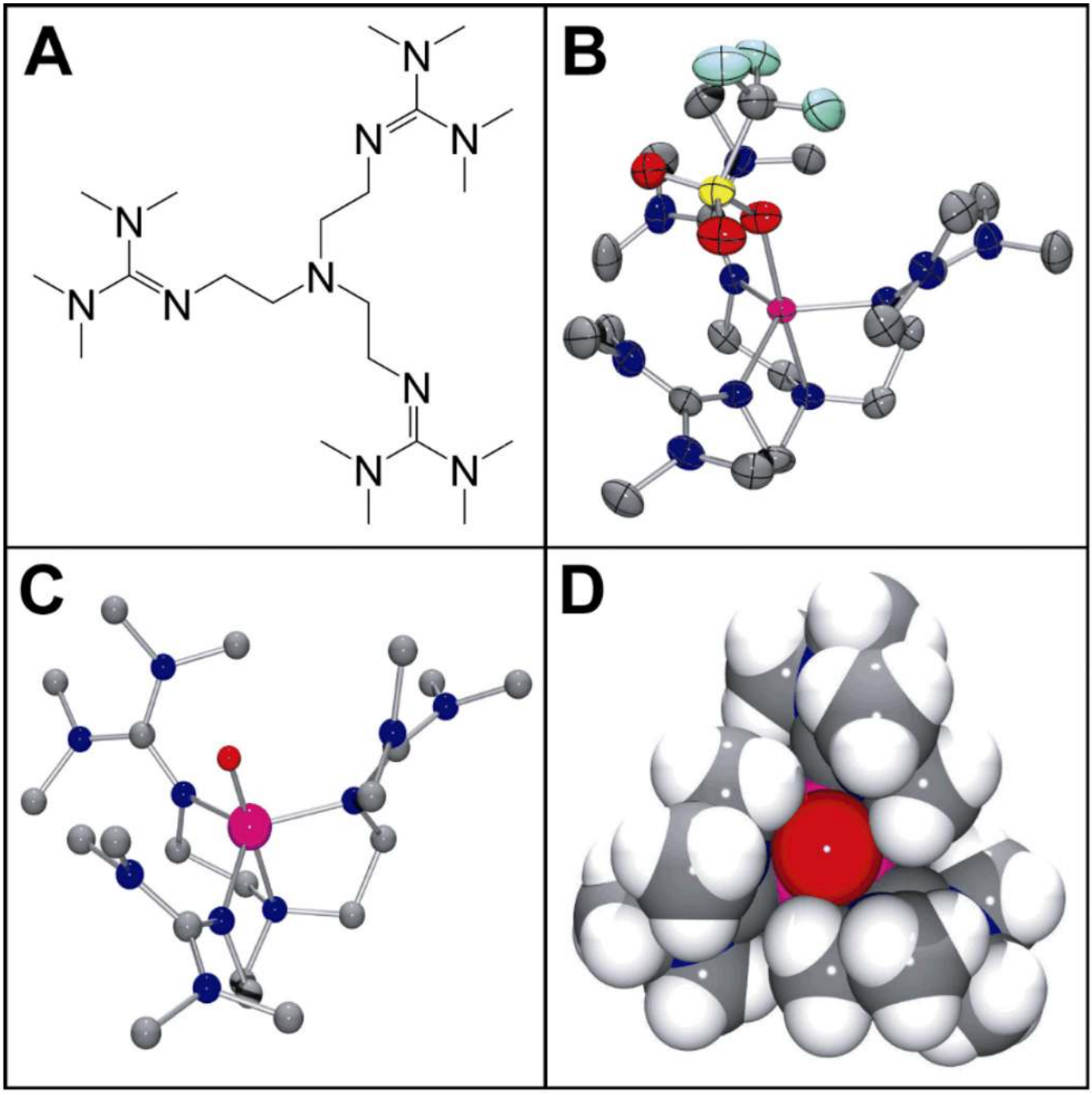

Figure 1.

(**A**) Schematic structure of the TMG_3tren ligand. (**B**) Thermal ellipsoid drawing of $[Fe^{II}(TMG_3tren)(OTf)]^+$ (**2**), showing 50% probability ellipsoids. Hydrogen atoms have been omitted for clarity. Selected bond distances (Å): Fe-O, 2.156(2); Fe-N_{axial}, 2.118(3); Fe-$N_{guanidine}$(ave), 2.094. (**C**) Ball-and-stick and (**D**) space-filling models of the DFT geometry optimized structure of **3**. Selected bond distances (Å): Fe=O, 1.648; Fe-N_{axial}, 2.121; Fe-$N_{guanidine}$(ave), 2.034. Atom color scheme: C, gray; N, blue, O, red; S, yellow; F, light blue; Fe, magenta.

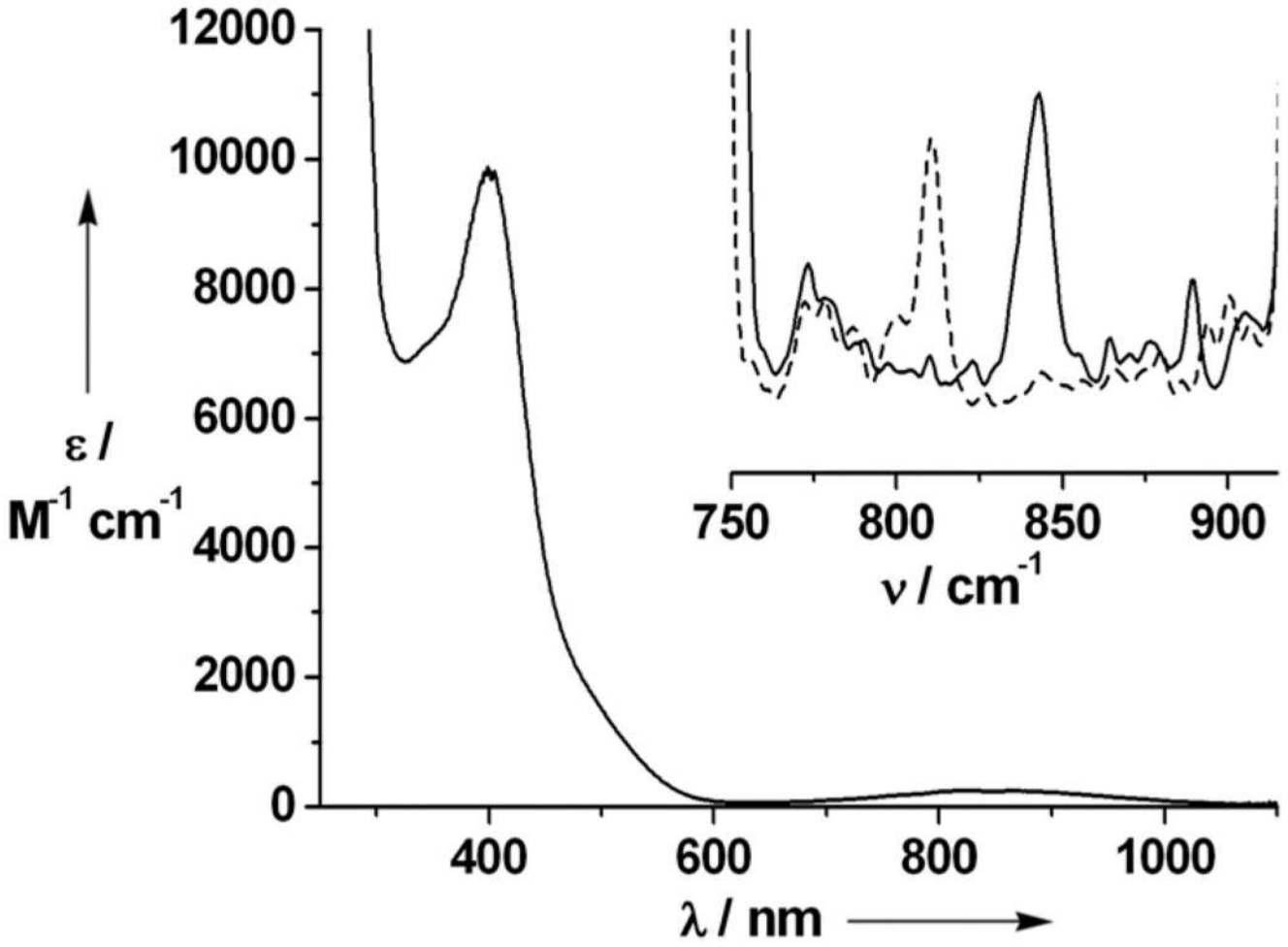

Figure 2.

Main: electronic spectrum of **3** in CH_3CN solution. Inset: resonance Raman spectra (λ_{ex} = 514.5 nm, power = 10 mW) of ^{16}O-**3** (solid line) and ^{18}O-**3** (dashed line) recorded in frozen CH_3CN solution.

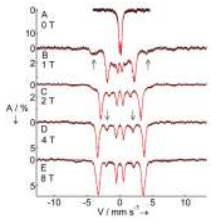

Figure 3.

4.2 K Mössbauer spectra of **3** in CH_3CN recorded in parallel applied magnetic fields, B, as indicated. Downward arrows indicate nuclear $\Delta m = 0$ transitions of the $M_S = 0$ ground state spectrum. Upward arrows mark outer absorption features of the spectrum associated with the $M_S = -1$ excited state. Solid lines are spectral simulations using the parameters listed in Table 1 with the $S = 2$ spin Hamiltonian $H = D(S_z^2 - 2) + E(S_x^2 - S_y^2) + 2\beta\, \boldsymbol{S}\cdot\boldsymbol{B} + \boldsymbol{S}\cdot\boldsymbol{A}\cdot\boldsymbol{I} - g_n\beta_n\, \boldsymbol{B}\cdot\boldsymbol{I} + H_Q$. In **B**, **C** and **D** a high-spin Fe^{III} impurity, representing 12% of the iron, has been subtracted from the raw data. In **E**, this impurity has not been subtracted and exhibits weak absorption bands at ~−6.5 and ~+7 mm/s.

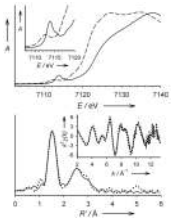

Figure 4.
Top: X-ray absorption edge spectra of **2** (– – –) and **3** (——). The inset shows an expansion of the pre-edge region. Bottom: Fe K-edge unfiltered EXAFS data ($k^3\chi(k)$, inset) and the corresponding Fourier transform of **3**. Experimental data are shown with dotted (•••) lines and fits with solid (——) lines. Please see Supporting Information for further details of the EXAFS analysis.

Table 1

Spectroscopic parameters of selected oxoiron(IV) complexes.

Complex	*S*	λ_{max} (nm)	$\nu_{Fe=O}$ (cm^{-1})	*D* (cm^{-1})	*E/D*	$A_{x,y,z}/g_n\beta_n$ (T)	ΔE_Q (mm/s)	η	δ (mm/s)	E_0 (eV)	Pre-edge area
3 (exp)	2	400	843	5.0(3)	0.02(1)	−15.5(4), −14.8(4), −28.0(8)	−0.29(3)	0	0.09(1)	7123.2	27
3 (DFT)[a]	2	-	-	-	-	−15, −15, −27.6	−0.49	0.02	0.11	-	-
TauD-**J**[b]	2	318	821	10.5	0.01	−18.4, −17.6, −31.0	−0.9	0	0.30	7123.8[d]	not reported
1[c]	2	320	-	9.7	0	−20.3, −20.3, nd	−0.33	0	0.38	7126	60–70
4[c]	1	820	834	29	0	−22.6, −18.3, −2.9	1.24	0.5	0.17	7124.5	32.8

[a] Calculated *A*-tensor was obtained by taking the experimentally determined A_{iso} = −19.4 T and adding the spin-dipolar term obtained from DFT.

[b] Data from references 2a and 15.

[c] **1** = $[Fe^{IV}(O)(OH_2)_5]^{2+}$ from reference 8; **4** = $[Fe^{IV}(O)(TMC)(NCCH_3)]^{2+}$ (TMC = 1,4,8,11-tetramethylcyclam) from reference 4 and 16.

[d] Assuming an Fe foil reference *E* of 7112.0 eV.

Table 2

Second-order rate constants (k_2) for oxidation reactions of Fe^{IV}=O complexes.

Complex	k_2 (M^{-1} s^{-1}) in CH_3CN at −30°C		
	PPh_3	DHA	CHD
3	1.1	0.090	1.2
4	0.22	0.016	0.018
5	1.5	2.0	1.3